ACS Catalysis

pubs.acs.org/acscatalysis Research Article

Competitive Photo-Oxidation of Water and Hole Scavengers on Hematite Photoanodes: Photoelectrochemical and Operando Raman Spectroelectrochemistry Study

Vivek Ramakrishnan, Anton Tsyganok, Elena Davydova, Mariela J. Pavan, Avner Rothschild, and Iris Visoly-Fisher*

Cite This: *ACS Catal.* 2023, 13, 540−549 Read Online

ACCESS | Metrics & More | Article Recommendations | Supporting Information

ABSTRACT: Hematite (α-Fe_2O_3) is one of the most studied photoanode materials due to its stability in alkaline electrolytes and visible light absorption. However, its reported performance lags significantly behind its theoretical limit. Toward determining routes for efficient photo-oxidation on hematite, we investigated the role of hole-trapping surface states as reaction intermediates using sacrificial reductant reagents as hole scavengers, H_2O_2 and FeCN. Photoelectrochemical characterization at low scavenger concentrations and intermediate potentials, as opposed to previous studies at high scavenger concentrations, has shown the reaction mechanism to include competitive photo-oxidation between water molecules and the hole scavengers, similar for both H_2O_2 and FeCN. Using operando Raman spectroelectrochemistry, we show similar transient features for both scavengers, interpreted as scavenger adsorption to a two-site reaction intermediate participating in the photogenerated hole transfer of water photo-oxidation, hence the competition. These findings strengthen the significance of hole-trapping surface states for water photo-oxidation on hematite and the previously suggested two-site reaction pathway for efficient hole transfer in this reaction. A better understanding of the mechanisms of photoelectrochemical water splitting can assist in improving the efficiency of solar hydrogen production.

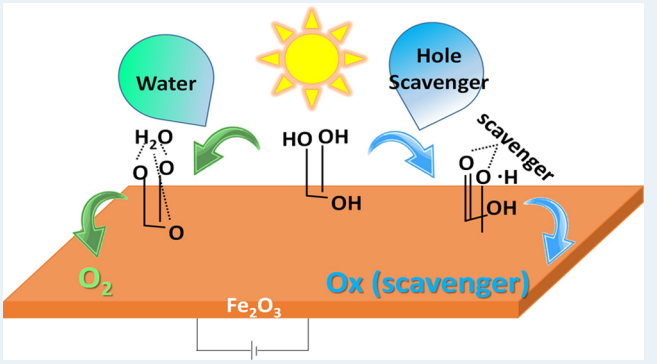

KEYWORDS: *hematite, operando Raman spectroelectrochemistry, hole scavenger, surface states, photo-oxidation*

INTRODUCTION

Photoelectrochemical (PEC) water splitting can generate clean fuels utilizing renewable resources: sunlight and water. A better understanding of the factors affecting the mechanisms of PEC water splitting can assist in improving the efficiency of PEC cells for solar to fuel conversion. Hematite (α-Fe_2O_3) is one of the most studied photoanode materials for solar-driven water photo-oxidation due to its stability in alkaline electrolytes, favorable alignment of its valence band with the water oxidation potential, and visible light absorption. A theoretical photocurrent limit of 12.6 mA/cm^2 was predicted based on its absorption edge (~600 nm),[1] but the maximal photocurrent reported for champion hematite photoanodes (~6 mA/cm^2 at the reversible potential for water oxidation, 1.23 V_{RHE})[2] is less than half of this limit. Different factors have been suggested to account for the underperformance of hematite photoanodes, including a short lifetime of the photogenerated minority charge carriers (i.e., holes) that leads to a short diffusion length of only 2−4 nm,[1,3−10] noncontributing light absorption due to localized d−d transitions,[11−13] and surface recombination of electrons with photogenerated holes trapped in surface states known as intermediates of the water photo-oxidation reaction.[6,14] This work investigates the interaction of these intermediates with sacrificial reductant reagents that are often used as hole scavengers to discern between bulk and surface electron−hole recombination losses.[15]

The fate of photogenerated holes trapped in surface states that serve as intermediates of the water photo-oxidation reaction plays a major role in the photoconversion efficiency on hematite and other metal-oxide photoanodes. To minimize photocurrent and overpotential losses, the lifetime of the surface-trapped photo-holes should be long enough to enable completing the multistep water photo-oxidation reaction before recombination with electrons takes place.[16] Sacrificial reductant reagents such as H_2O_2 or $[Fe(CN)_6]^{3-/4-}$ (herein

Received: June 12, 2022
Revised: December 7, 2022

https://doi.org/10.1021/acscatal.2c02849
ACS Catal. 2023, 13, 540−549

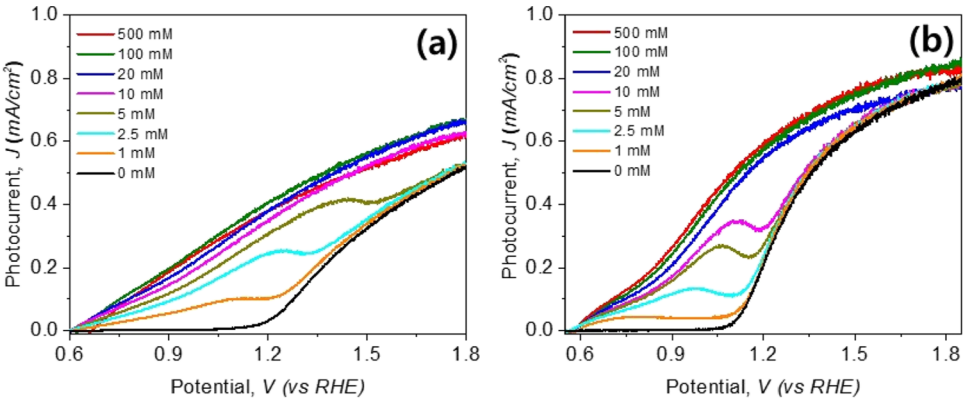

Figure 1. Net photocurrent voltammograms with varying concentrations of (a) H_2O_2 and (b) FeCN in an alkaline aqueous electrolyte (1 M NaOH, pH 13.6). Calculated from the data in Figures S2 and S3.

denoted as FeCN) are often used as hole scavengers to collect the photo-holes arriving at the surface faster than the water photo-oxidation reaction so as to avoid surface recombination and discern between surface and bulk recombination losses.[15,17−19] H_2O_2 is a sacrificial reductant that decomposes photolytically during measurement by injecting electrons to the illuminated photoanode. In the potential range where water photo-oxidation occurs, H_2O_2 can be oxidized, but it cannot be reduced. Therefore, it serves as a selective probe for the flux of photo-holes arriving at the surface. In contrast, FeCN, a one-electron redox couple, is a regenerative redox shuttle that can carry ambipolar (photo)currents.

Comparison of PEC measurements of thin-film hematite photoanodes with large concentrations of H_2O_2 and FeCN reveals that the photocurrents are nearly similar in both hole scavengers (Figure S1, Supporting Information). Interestingly, overlaying this photocurrent with the water photo-oxidation voltammogram (without sacrificial reagents) shows good correlation at high potentials, upon a cathodic potential shift of ∼270 mV (Figure S1D), presumably associated with the surface potential of oxidized intermediate states that play a pivotal role in water photo-oxidation.[20] This suggests that both hole scavengers utilize a similar mechanism for hole extraction from the intermediate surface states participating in water photo-oxidation. However, the details of this mechanism could not be characterized with these large concentrations.

We have recently measured the performance of a thin-film hematite photoanode in varying concentrations of H_2O_2.[21] Through analysis and simulations, we attributed the behavior to competition for surface sites between water and H_2O_2 photo-oxidation, which could not be observed at large H_2O_2 concentrations. We postulated a mechanism for H_2O_2 photo-oxidation that involves two reaction sites as in Langmuir−Hinshelwood (L−H) reactions,[21] in contrast with a mechanism that involves a single reaction site as in Eley−Rideal (E−R) reactions typically assumed for water photo-oxidation.[22] When the photo-oxidation reaction splits into two sites, the collection of photogenerated holes by the oxidized species can be enhanced by leveling the potential of the reaction intermediate steps, hence decreasing energy barriers. We suggested that the concerted interaction of two surface intermediates might lead to improved photoelectrode performance,[21] in agreement with other works.[17,23−25] Herein, the robustness of these findings is experimentally substantiated by demonstrating a similar competition for surface sites participating in water photo-oxidation applied by a different hole scavenger, namely, FeCN.

Operando spectroelectrochemistry studies were proven to be useful for studying photoelectrochemical reactions by detecting the reaction intermediates.[22,26−28] Operando Raman spectroscopy has several advantages, including the ability to probe the photoelectrode surface through aqueous solutions and sensitivity to functional groups containing lightweight elements such as H. Potential-dependent operando Raman spectroscopy was employed to study the intermediates formed during the reversible reduction of α- and γ-FeOOH to $Fe(OH)_2$.[29] Operando Raman spectroscopy was also utilized to follow intermediate species and surface changes in various electro-catalysts for the OER in the dark;[25,30−39] however, we could not find published works describing operando Raman characterization of water photo-oxidation under illumination, as described herein. We used operando Raman spectroelectrochemistry to identify the reaction intermediates/surface sites involved in the competition between water- and hole scavengers' photo-oxidation.

RESULTS AND DISCUSSION

Photoelectrochemical Characterization. We first examined the photocurrent voltammograms in alkaline (1 M NaOH, pH 13.6) electrolytes with varying concentrations of H_2O_2 or FeCN. The inspiration for this came from our previous study where the competitive coexistence of two reaction paths of H_2O and H_2O_2 photo-oxidation was observed at intermediate H_2O_2 concentrations (2.5−10 mM) and intermediate potentials (0.8−1.3 V_{RHE}) around the onset of water photo-oxidation. This resulted in nonmonotonous photocurrent voltammograms displaying negative differential resistance (NDR) typical of competing mechanisms with different time scales and a hysteresis loop when the potential was swept back and forth.[21] These results were reproduced herein, as shown in Figure 1a. Figure 1b shows the photocurrent linear sweep voltammogram in alkaline electrolytes with varying concentrations of FeCN. The onset of water photo-oxidation (without FeCN, black curve) is at ∼1.1 V_{RHE}, while the onset of FeCN photo-oxidation is at ∼0.6 V_{RHE} (0.5 M FeCN, red curve). At FeCN concentrations of ≥20 mM, a monotonic increase in the photocurrent with increasing potentials is noted, attributed to FeCN photo-oxidation at intermediate potentials up to ∼1.1 V_{RHE} and the dominating water photo-oxidation at higher potentials. However, at low concentrations (1−10 mM), a nonmonotonic behavior with

https://doi.org/10.1021/acscatal.2c02849
ACS Catal. 2023, 13, 540−549

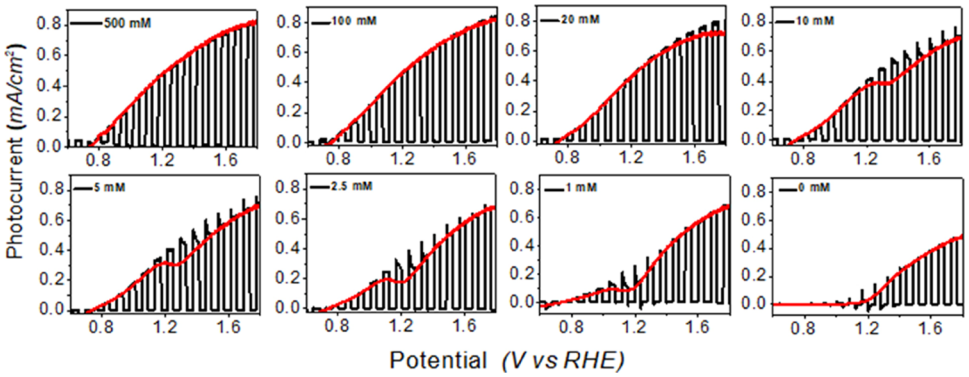

Figure 2. Photocurrent voltammograms with varying concentrations of FeCN in an alkaline aqueous electrolyte (1 M NaOH, pH 13.6) under chopped illumination (black) overlaid with LSV measurements at constant illumination (red).

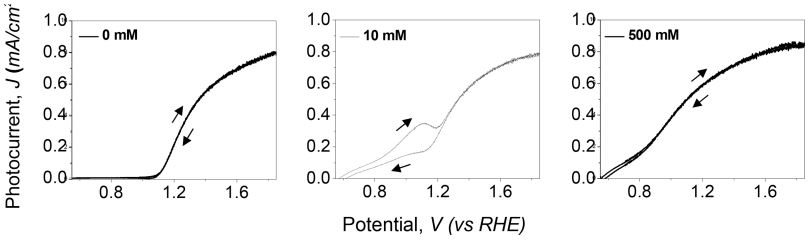

Figure 3. Forth and back photocurrent linear sweep voltammograms at varying concentrations of FeCN in an alkaline aqueous electrolyte (1 M NaOH, pH 13.6) on hematite, showing hysteretic behavior at an intermediate FeCN concentration.

NDR is observed in the intermediate potential range, in accordance with that observed with H_2O_2 (Figure 1a). The negative slope is followed by a sharp rise near the onset of water photo-oxidation, with the photocurrent coinciding with that of pure water photo-oxidation (black curve) at larger potentials. The coexistence of FeCN and water oxidation at these conditions was verified by the analysis of the Faradaic efficiency (Table S1, Supporting Information) and was also previously suggested.[40]

The NDR peak potential, indicating the transition from the FeCN-limited photocurrent at low potentials to the water photo-oxidation current at high potentials, shifts anodically with increasing FeCN concentrations, indicating a change in the rate of FeCN photo-oxidation. Photocurrent voltammograms measured at various scan rates yielded similar NDR but with a shift of the NDR peak to larger potentials with increased scan rates, indicating the quasi-reversible nature of the FeCN photo-oxidation reaction (Figure S4ai). Plotting the peak currents as a function of the square root of the scan rate indicates a diffusion-controlled process (Figure S4aii, iii). The FeCN cathodic (reduction) current upon reverse scanning peaked around 0.6 V_{RHE} and was insensitive to illumination, as expected from the n-type nature of the hematite photoanode (Figure S4bi, ii). Possible alternative artifacts, such as the effect of the FTO substrate or hematite decomposition, were ruled out as causes of this behavior by control experiments (Figures S5 and S6).

To shed further light on the competition between water and FeCN photo-oxidation, photocurrent voltammograms were measured under chopped illumination. Figure 2 shows the overlaid photocurrent curves measured under chopped and constant illumination. At zero or low FeCN concentrations, where water photo-oxidation is the dominating reaction, anodic photocurrent transient spikes can be observed upon light turn-on. Such spikes were previously attributed to the recombination of surface-trapped holes with conduction band electrons.[17] Cathodic transients upon light turn-off are also noted at zero or low scavenger concentrations and are related to the reduction of surface-trapped holes (Figure S7b). The steady-state anodic photocurrents under chopped illumination traced the NDR pattern at intermediate FeCN concentrations (1−2.5 mM), verifying that this behavior is a steady state rather than the transient pattern. This behavior was similar to that observed in the same photoanode when probed with H_2O_2 (Figure S7).

The coexistence of competing reaction pathways was shown to lead to hysteresis of the photocurrent voltammograms at intermediate potentials and H_2O_2 concentrations (Figure S8b and ref 21). The hysteresis was predicted from bistable solutions of the kinetic model in ref 21, in a given combination of potential and concentration ranges, and is related with the coexistence of competing oxidation reactions. A similar behavior is observed here for FeCN (Figure 3), suggesting similar competition between FeCN and water photo-oxidation reactions. At very low FeCN concentrations, water photo-oxidation is the dominant reaction, whereas at high concentrations, FeCN photo-oxidation prevails at low and intermediate potentials. At intermediate concentrations, there is coexistence of both processes, competing for surface states and photogenerated holes, leading to hysteretic behavior as theoretically predicted and experimentally verified for H_2O_2 in our previous study.[21] A possible mechanism is proposed below to account for such competition.

Operando Raman Spectroelectrochemistry. The photoelectrochemical voltammetry results presented above substantiate the robustness of the competition for surface sites between water and hole scavenger's photo-oxidation by demonstrating similar phenomena with H_2O_2 and FeCN hole scavengers. We note that a similar photoelectrochemical voltammetry behavior does not necessarily mean the two hole

https://doi.org/10.1021/acscatal.2c02849
ACS Catal. 2023, 13, 540−549

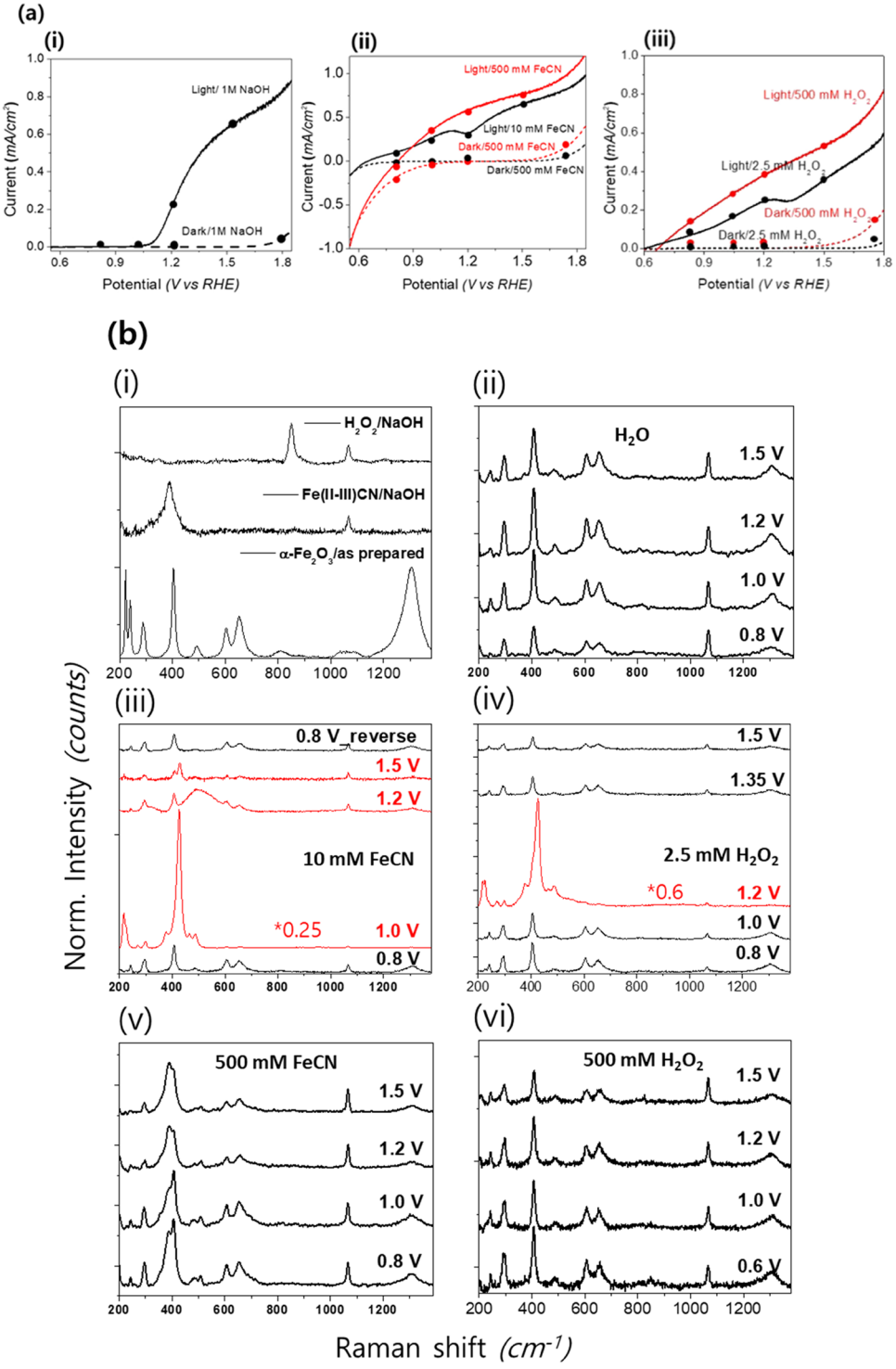

Figure 4. Operando Raman spectroelectrochemistry measurements with and without hole scavengers: (a) linear sweep voltammograms (full lines—under illumination, dashed lines—in the dark) with full circles indicating the potentials where operando Raman spectroelectrochemistry measurements were taken in (i) 1 M NaOH without sacrificial reagents, (ii) 1 M NaOH with 10 or 500 mM FeCN (black and red curves, respectively), (iii) 1 M NaOH with 2.5 or 500 mM H_2O_2 (black and red curves, respectively). (b) (i) Ex situ Raman spectra of the dry hematite photoanode and 1 M NaOH solution with 500 mM FeCN or H_2O_2 on an inert substrate (bottom, middle, and top curves, respectively); (ii–vi) Operando Raman spectroelectrochemistry measured at various potentials under illumination with aqueous alkaline electrolytes (1 M NaOH) containing (ii) H_2O only, (iii) 10 mM FeCN (the spectrum measured at 1 V is reduced by a factor of 0.25 to allow comparison with other spectra), (iv) 2.5 mM H_2O_2 (the spectrum measured at 1.2 V is reduced by a factor of 0.6 to allow comparison with other spectra), (v) 500 mM FeCN, and (vi) 500 mM H_2O_2. Transient spectra are indicated in red. The spectra were vertically stacked for clarity. Potentials are indicated vs RHE.

scavengers have the same oxidation mechanism; therefore, we used operando Raman spectroelectrochemical characterization to further compare these mechanisms. Operando Raman spectroelectrochemistry was then used to identify the reaction intermediates/surface sites involved in the competition between water- and hole scavengers' photo-oxidation. Raman

https://doi.org/10.1021/acscatal.2c02849
ACS Catal. 2023, 13, 540−549

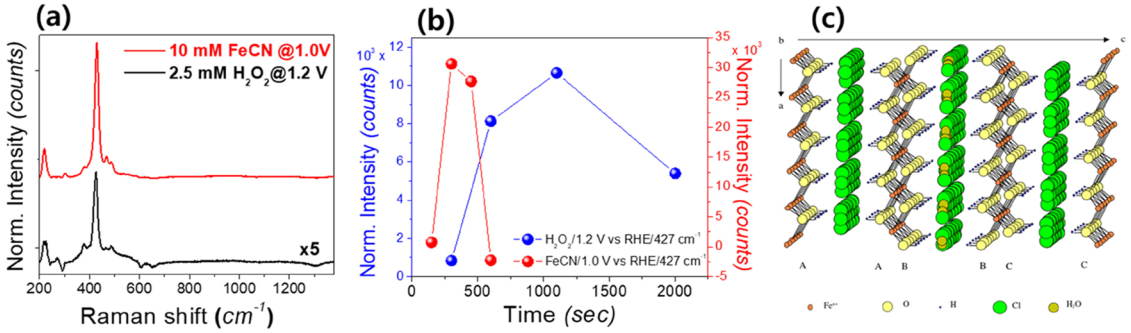

Figure 5. (a) Difference spectra obtained by the subtraction of operando Raman spectra of 10 mM FeCN at 1.0 V_{RHE} and 2.5 mM H_2O_2 at 1.2 V_{RHE} from the respective spectra at 0.8 V_{RHE}. (b) Time-dependent rise and decay of the transient peak intensity at 427 cm^{-1} measured with operando Raman spectroelectrochemistry of 10 mM FeCN at 1 V_{RHE} and 2.5 mM H_2O_2 at 1.2 V_{RHE}. The electrolyte in all cases was 1 M NaOH. (c) Crystal structure of GR (reproduced from ref S6, under the Creative Commons CC0 License).

spectra were collected at different photocurrent regimes in the photoelectrochemical voltammetry measurements: hole scavenger photo-oxidation-dominated range (low potentials and/or high scavenger concentration), water photo-oxidation-dominated range (high potentials and/or no scavenger), and bistable range of competing reactions (intermediate potentials and scavenger concentrations). Figure 4a shows the points on the dark and light voltammograms measured with and without FeCN and H_2O_2 hole scavengers where operando Raman spectra were recorded (see also Table S2).

The Raman spectrum of a dry hematite photoanode (Figure 4b(i), bottom spectrum) shows peaks at 227, 243, 292, 299, 407, 495, 606, 655, 810 (broad), ~1050 (broad), and 1305 cm^{-1}, almost all characteristic of hematite, except for the peaks at 299 and 655 cm^{-1} which correspond to Fe_3O_4.[41,42] As XRD has not shown Fe_3O_4 in similar hematite photoanodes,[43] this may indicate its presence at small content on or near the surface. The electrolytes (1 M NaOH with 500 mM H_2O_2 or with 500 mM FeCN) background spectra showed peaks at 389, 850, and 1066 cm^{-1} (Figure 4b(i), top and middle spectra, respectively), arising from FeCN, H_2O_2, and NaOH, respectively.[44] Operando Raman spectra were recorded for the hematite photoanode under bias potential and illumination (532 nm laser) in reflectance configuration (Figure S9) through a thin (2.4 mm) electrolyte layer (Figure 4b(ii–vi)). The corresponding spectra measured in the dark are shown in Figure S10.

In operando measurements of water photo-oxidation (without sacrificial reagents), no significant changes in the Raman spectra were observed at different potentials (Figure 4b(ii)), indicating that the reaction intermediates are poor Raman scatterers in the measured spectral range or undetectable due to their low concentration/short lifetimes. At low (10 mM) FeCN concentration, a set of additional peaks were observed at and above 1 V_{RHE} (Figure 4b(iii), red spectra), which disappeared at potentials above the onset of water oxidation in the dark (1.5 V_{RHE}) or when the potential was reverted back to 0.8 V_{RHE}. The new peaks were at 217, 269, 377, 427, 465, 490 (broad) cm^{-1}, of which the peaks at 217 and 427 cm^{-1} were of exceptional intensity. We assign these peaks to long-lived, metastable intermediates of FeCN photo-oxidation. At high (500 mM) FeCN concentration, no bias-dependent changes were observed except for a slight relative increase in the FeCN-related peak intensity at 389 cm^{-1} with increasing potentials (Figure 4b(v)). All the peaks observed at this concentration were related to hematite or to the electrolyte [see Figure 4b(i)]. We suppose that the reaction intermediates are short-lived at high concentration due to removal of the reactant diffusion limitations.

A matching behavior was observed in the presence of H_2O_2. Similar to the additional Raman peaks observed with 10 mM FeCN (Figure 4b(iii)), additional prominent peaks were observed with 2.5 mM H_2O_2 (at 1.2 V_{RHE}) at 217 and 427 cm^{-1} (Figure 4b(iv)). In both measurements, with FeCN and H_2O_2, the potentials where the additional Raman peaks were observed were at the rise of the NDR peak (1 V_{RHE} for FeCN, 1.2 V_{RHE} for H_2O_2, see Figure 4a(iii) and (iv), respectively), i.e., where both water and hole scavenger photo-oxidation reactions coexist. The additional Raman peaks disappeared at larger potentials also in the case of H_2O_2. Figure 5a shows the difference spectra resulting from subtracting the respective spectra measured at 0.8 V_{RHE} (where no additional peaks are observed) from those measured at 1.0 V_{RHE} with 10 mM FeCN or at 1.2 V_{RHE} with 2.5 mM H_2O_2 (where the additional peaks of interest were observed, Figure 4b(iii, iv)). The difference spectra show that the additional peaks had similar characteristics for both scavengers (FeCN and H_2O_2), hinting to the similar photo-oxidation mechanism of either hole scavenger. The similar spectroelectrochemical results obtained for both hole scavengers, in addition to the similar photoelectrochemical voltammetry results described above, further support the robustness of the competition for the surface states participating in water photo-oxidation, which is common to both cases.

The spectra showing additional Raman peaks (red spectra in Figure 4biii, iv), observed at low hole scavenger concentration and intermediate potentials, are termed "transient" as the additional peaks disappear at higher or lower potentials and concentrations. The ~0.2 V difference in the potential at which the transients appear between both scavengers (Figure 4biii, iv) is well correlated with the NDR peak shift in the photocurrent density voltammograms (Figure 4aii, iii). The "transient" spectra (for both FeCN and H_2O_2) were also found to vary with time as discussed below. To affirm the assignment of the additional peaks to surface intermediates of the photo-oxidation reaction, operando experiments were repeated in the dark. No additional peaks were observed with H_2O_2 or FeCN in the dark (Figure S10). Potential artifacts affecting the transient Raman spectra, such as those originating from the substrate (Pt/Si) and the bulk electrolyte constituents, were ruled out by control experiments (Figure S11).

https://doi.org/10.1021/acscatal.2c02849
ACS Catal. 2023, 13, 540−549

The transient peaks at 427 and 490 cm^{-1} were assigned to Fe^{2+}−OH and Fe^{3+}−OH stretch modes, respectively, in a green rust (GR)-like complex[45] (Figure 5c). A GR-like complex is a positively charged layered complex of iron atoms at oxidation states of +2 and +3 and hydroxy anions, with characteristic Raman peaks at 433 and 503 cm^{-1}.[45−49] The slight wavenumber shift in our case could be attributed to the different counter anions of the coordinated scavengers. GR layers were reported to be highly susceptible to further oxidation to goethite (α-FeOOH) in alkaline conditions.[50] The adsorption of $[Fe(CN)_6]^{3-}$ to goethite (α-FeOOH) has been well studied, and at alkaline conditions, it tends to form an outer-sphere complex with weak van der Waals forces.[51−53] It was also reported that $[Fe(CN)_6]^{4-}$ sorbs more strongly on Fe oxides than does $[Fe(CN)_6]^{3-}$,[53] supporting the planar dense surface coordination of both species which can resemble GR. The other transient peaks observed for both scavengers at 217, 270, 377, and 465 cm^{-1} are hypothesized to originate from surface iron oxyhydroxide (FeOOH).[29,42,54,55] The formation of the metal oxyhydroxide moiety has been previously reported to be involved in water[26] and H_2O_2[21] photo-oxidation on hematite.

To further study the nature of the transient Raman peaks observed at intermediate potentials and low scavenger concentrations (2.5 mM FeCN, 10 mM H_2O_2), the intensity of the peaks was followed as a function of time by repeated Raman measurements, while other conditions were kept constant (Figure S12). Figure 5b shows the temporal intensity changes of the transient peak at ∼427 cm^{-1} for both FeCN and H_2O_2. The peaks were found to persist for hundreds s, too long to reflect on the intermediates' lifetime. Such long persistence is probably related to the consumption of the reactant yielding this intermediate, i.e., the scavenger, which is at low concentration. Moreover, comparing the peaks of both hole scavengers, we observe that the transient peak of FeCN (at 1.0 V_{RHE}) was of three times larger intensity than that measured for H_2O_2 (at 1.2 V_{RHE}, Figure 4biii, iv) and grows and decays ∼3 times faster (the time until the maximum peak intensity is 300 s for FeCN compared to ∼1100 s for H_2O_2, Figure 5b). Both these observations probably reflect the ×4 difference in scavenger concentrations. This further demonstrates the similarity in transient behavior between both scavengers, possibly indicating its common nature, despite the different number of holes involved in the scavengers' photo-oxidation.

Suggested Mechanism. Though the water photo-oxidation mechanism on hematite photoanodes is still under debate,[24,26,57] a common feature of all the proposed reaction pathways is that they involve a sequence of four OH^--coupled hole transfer steps whereby surface adsorbates on Fe reaction centers are deprotonated. As such, they accommodate the holes trapped in the reaction intermediates while maintaining charge neutrality. The most popular pathway proposes a sequence where the adsorbate changes from −OH to =O to −OOH and back to −OH.[58] Using *operando* infrared spectroscopy measurements combined with isotopically labeled water, Zandi and Hamann[22] provided spectroscopic evidence for an oxygen-containing surface species generated during water photo-oxidation on hematite and assigned it to Fe^{4+}=O intermediates. Other intermediates such as Fe−OH and −OOH species were suggested by other researchers.[59,60] Durrant and co-workers suggested different reaction pathways depending on hole density, viz., first (at low illumination intensity)- and third (at high illumination intensity)-order reactions.[26,61,62] The latter reaction mechanism involves the consecutive oxidation of a complex of adjacent two surface sites, a Fe(OH)−O−Fe(OH) dimer, in accordance with our previous study of the mechanism of H_2O_2 photo-oxidation on hematite that proposed a two-site pathway.[21] As our experimental conditions correspond to high illumination intensity, we propose a two-site hole-scavengers' photo-oxidation mechanism wherein the reaction intermediates of the water- and hole-scavengers' photo-oxidation reactions compete for surface sites and photo-holes, as described in the following.

Due to the similarity in the Raman spectra measured during the photo-oxidation of both H_2O_2 and FeCN hole scavengers (Figure 4biii, iv), we postulate that a similar reaction intermediate facilitates the hole transfer to both scavengers. It should be noted that in an alkaline aqueous solution, H_2O_2 is deprotonated to yield OOH^-,[21,63] whose oxidation involves an additional hole transfer compared to FeCN. Based on the identification of the transient Raman peaks as being related to GR-like species, a layered complex of Fe^{2+}, Fe^{3+} and OH^-, and to FeOOH (see above), we propose the two-site intermediate complex presented in Figure 6.

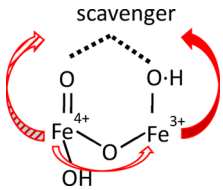

Figure 6. Proposed reaction intermediate for the photo-oxidation of dilute hole scavengers (FeCN and H_2O_2) at intermediate potentials. The red arrows show the suggested hole transfer pathway: full arrow—from the Fe^{3+} surface site to the oxidizing scavenger (FeCN or H_2O_2); striped arrow—from Fe^{4+} to the oxidizing H_2O_2 (only); and hollow arrow—the subsequent hole transfer from the oxidized Fe^{4+} to the Fe^{3+} surface site.

This complex consists of the hole scavenger physically adsorbed to the one-hole oxidized two-site complex suggested in,[26] probably by the Coulomb attraction of the single hole-charged surface species with the negatively charged scavenger moiety. We assume that this electrostatic binding stabilizes this complex and prolongs its lifetime to make it Raman-detectable. The photogenerated holes presumably transfer to the oxidizing scavenger via the Fe^{3+}OH site, i.e., Fe^{3+}OH loses a hole and becomes Fe^{2+}OH. Fe^{2+} is then oxidized by hole transfer from the adjacent (formerly photo-oxidized) Fe^{4+}, suggesting the role of the concerted two-site reaction. Indeed, at 1.2 V_{RHE}, where the FeCN photo-oxidation decays (Figure 4aii), a broad peak was noted at ∼490 cm^{-1} (associated with Fe^{3+}−OH) with the 427 cm^{-1} (associated with Fe^{2+}−OH) and other transient peaks (associated with FeOOH) diminished (Figure 4biii). In the case of H_2O_2 photo-oxidation, an additional photogenerated hole is transferred to the oxidizing species via the Fe^{4+} moiety, as in water photo-oxidation. It is noted that the proposed intermediate (Figure 6) is compatible with our previously suggested mechanism for H_2O_2 photo-oxidation based on PEC voltammetry measurements, showing competing H_2O_2 and H_2O photo-oxidation reactions presumably related to a surface complex of Fe=O and Fe−OH···scavenger.[21] The current findings therefore provide further support to the model suggested based only on PEC measurements.

https://doi.org/10.1021/acscatal.2c02849
ACS Catal. 2023, 13, 540−549

Equations 1−16 describe the proposed competing photo-oxidation reaction mechanisms of water and both hole scavengers. We note that these mechanisms are speculated based on previous studies and the operando Raman results described herein, and alternative mechanisms cannot be ruled out. According to Durrant and co-workers,[26] at high light intensities, the water photo-oxidation mechanism is described by eqs 1−8 (the subscript "s" denotes a surface-bound species):

$$[Fe^{3+}OH]-O-[Fe^{3+}OH(OH)]_s + h^+ \rightarrow [Fe^{3+}OH]-O-[Fe^{4+}{=}O(OH)]_s + H^+ \quad (1)$$

$$[Fe^{3+}OH]-O-[Fe^{4+}{=}O(OH)]_s + h^+ \rightarrow [Fe^{4+}{=}O]-O-[Fe^{4+}{=}O(OH)]_s + H^+ \quad (2)$$

$$[Fe^{4+}{=}O]-O-[Fe^{4+}{=}O(OH)]_s + h^+ \rightarrow [Fe^{4+}{=}O]-O-[Fe^{5+}{=}O(O)]_s + H^+ \quad (3)$$

$$[Fe^{4+}{=}O]-O-[Fe^{5+}{=}O(O)]_s + H_2O \rightarrow [Fe^{4+}{=}O]-O-[Fe^{5+}{=}O](O)(OH_2)]_s \quad (4)$$

$$[Fe^{4+}{=}O]-O-[Fe^{5+}{=}O(O)(OH_2)]_s \rightarrow [Fe^{3+}OOH]-O-[Fe^{4+}{=}O(OH)]_s \quad (5)$$

$$[Fe^{3+}OOH]-O-[Fe^{4+}{=}O(OH)]_s \rightarrow [Fe^{3+}OO^{\cdot}]-O-[Fe^{3+}OH(OH)]_s \quad (6)$$

$$[Fe^{3+}OO^{\cdot}]-O-[Fe^{3+}OH\ (OH)]_s + H_2O \rightarrow [Fe^{2+}OH_2]-O-[Fe^{3+}OH(OH)]_s + O_2 \quad (7)$$

$$[Fe^{2+}OH_2]-O-[Fe^{3+}OH(OH)]_s + h^+ \rightarrow [Fe^{3+}OH]-O-[Fe^{3+}OH(OH)]_s + H^+ \quad (8)$$

We propose that the FeCN photo-oxidation utilizes the product of reaction 1, thus competing with reaction 2 and the consecutive reaction steps:

$$[Fe^{3+}OH]-O-[Fe^{4+}{=}O(OH)]_s + [Fe^{2+}(CN)_6]^{4-} \rightarrow [Fe^{3+}OH]-O-[Fe^{4+}{=}O(OH)]^{\cdots}[Fe^{2+}(CN)_6]^{4-}{}_s \quad (9)$$

$$[Fe^{3+}OH]-O-[Fe^{4+}{=}O(OH)]^{\cdots}[Fe^{2+}(CN)_6]^{4-}{}_s \rightarrow [Fe^{2+}OH]-O-[Fe^{4+}{=}O(OH)]_s + [Fe^{3+}(CN)_6]^{3-} \quad (10)$$

$$[Fe^{2+}OH]-O-[Fe^{4+}{=}O(OH)]_s + H_2O \rightarrow [Fe^{3+}OH]-O-[Fe^{3+} - OH(OH)]_s + OH^- \quad (11)$$

H_2O_2 photo-oxidation utilizes a similar route, following its deprotonation in the alkaline electrolyte, as proposed in ref 21:

$$HOOH + OH^- \rightarrow HOO^- + H_2O \quad (12)$$

$$[Fe^{3+}OH]-O-[Fe^{4+}{=}O(OH)]_s + HOO^- \rightarrow [Fe^{3+}OH]-O-[Fe^{4+}{=}O(OH)]^{\cdots}HOO^-{}_s \quad (13)$$

$$[Fe^{3+}OH]-O-[Fe^{4+}{=}O(OH)]^{\cdots}HOO^-{}_s + h^+ \rightarrow [Fe^{3+}OH]-O-[Fe^{5+}{=}O(OH)]^{\cdots}HOO^-{}_s \quad (14)$$

$$[Fe^{3+}OH]-O-[Fe^{5+}{=}O(OH)]^{\cdots}HOO^-{}_s \rightarrow [Fe^{2+}OH]-O-[Fe^{4+}{=}O(OH)]^{\cdots}H^+{}_s + O_2 \quad (15)$$

$$[Fe^{2+}OH]-O-[Fe^{4+}{=}O(OH)]^{\cdots}H^+{}_s \rightarrow [Fe^{3+}OH]-O-[Fe^{3+}-OH(OH)]_s \quad (16)$$

The proposed mechanisms suggest the competition between the hole scavenger and water photo-oxidation to rely on utilizing the product of reaction (1) for hole transfer to the oxidizing species based on the identification of the participating reaction intermediates from Raman spectroelectrochemistry. Evidence for such competition by photoelectrochemical voltammetry and spectroelectrochemistry can be observed only when studying the photo-oxidation reactions at intermediate potentials and low hole scavenger concentrations, where neither photo-oxidation routes dominates but rather both coexist and compete with each other, as described above and in our previous work.[21] The difference between water- and scavenger-photo-oxidation lays in the hole transfer via $Fe^{3+}OH$ surface species, which does not occur in water photo-oxidation. This hole transfer is suggested to be enabled by the concurrent two-site binding of the scavenger molecule to $Fe^{3+}OH$ and $Fe^{4+}{=}O$. The significance of the current work is by demonstrating the similar behavior of both hole scavengers studied, H_2O_2 and FeCN, and by identifying the hematite species responsible for this similarity. This further strengthens the significance of hole-trapping surface species for water photo-oxidation on hematite[14,22,26,62,64,65] and the suggested two-site reaction pathway for efficient hole transfer in this reaction.[17,21,23,24]

SUMMARY AND CONCLUSIONS

The current work demonstrates the significance of hole scavenger studies at varying concentrations and potentials for determining hematite photoanode surface properties, in addition to the photoanode surface properties determined by studies at high scavenger concentrations. Photoelectrochemical characterization at low hole scavenger concentrations and intermediate potentials has shown similar competitive photo-oxidation on hematite photoelectrodes between both studied hole scavengers, namely, H_2O_2 and FeCN, and water. The competition for photogenerated holes and intermediate surface species results in NDR and hysteresis in the photocurrent voltammograms, in the presence of dilute hole scavengers and at intermediate potentials, near the photocurrent onset potential. The robustness of this phenomenon demonstrates the significant role played by the hole-trapping surface species for water photo-oxidation on hematite.

The photo-oxidation of both hole scavengers was further studied using operando Raman spectroscopy. Transient Raman features were detected with both hole scavengers on hematite at low scavenger concentrations and intermediate potentials, where competitive photo-oxidation was shown to occur under similar conditions in PEC voltammetry measurements. We interpret these transient spectroscopic signatures as being related with scavenger adsorption to the same two-site reaction intermediate participating in the (first) photogenerated hole transfer of water photo-oxidation, hence the competition. The

https://doi.org/10.1021/acscatal.2c02849
ACS Catal. 2023, 13, 540−549

understanding of the hole scavenger photo-oxidation mechanism, and its utilization of the same surface species participating in water photo-oxidation on hematite, sheds further light on the role of these surface species in water splitting toward performance optimization of hematite photoelectrodes.

METHODS

Photoanode Fabrication. Thin films of Sn-doped (1%) hematite (40 nm) were deposited on fluorine-doped tin oxide (FTO, 400−450 nm thickness, TEC15) or Pt (∼200 nm)-coated silicon (undoped, 510−540 mm thickness, <100> oriented, Shin-Etsu Chemical Co., Ltd.) substrates by pulsed laser deposition. Detailed preparation and structural characterization are reported elsewhere.[43]

PEC Measurements. All PEC measurements were carried out in an aqueous alkaline electrolyte of 1 M NaOH (J. T. Baker, electronic grade) in deionized water (J. T. Baker, HPLC grade), pH ∼13.6, under ambient conditions. Stock solutions of either scavenger (500 mM), H_2O_2 (Sigma Aldrich) or FeCN mixture (0.5 M $K_3Fe(CN)_6$ and 0.5 M $K_4Fe(CN)_6$, Carl Roth Chemicals, ACS, ≥99%), were prepared in 1 M NaOH and diluted with the same for varying concentrations ranging from 500 to 1 mM. Linear sweep voltammetry (LSV) and cyclic voltammetric (CV) measurements were carried out using the "Cappuccino cell"[7] and a three-electrode potentiostat (EC-Lab, SP-300, BioLogic) at a scan rate of 20 mV/s unless otherwise noted. The three-electrode configuration used a Pt coil (CH Instruments) as the counter electrode and Ag/AgCl (sat. KCl, BAS Inc.) as the reference electrode. All the LSV and cyclic voltammograms were converted to reversible hydrogen electrode scale (RHE) via the Nernst equation. The current density was calculated by dividing the measured current by the working electrode area (0.28 cm^2). The light source was a Xe lamp (Spectral Products, Model No. ASB-XE-175) with an intensity of 100 mW/cm^2. Since FeCN is colored, PEC measurements with this scavenger used back side illumination. The net photocurrent was calculated as the difference between the measured photocurrent and dark current (at the same potential) (Figures S2 and S3). Faradaic efficiency measurements were applied to the photoanode in the electrolyte solution of 1 M NaOH and 2.5 mM $K_4Fe(CN)_6$ at the potential range of 1.3−1.6 V vs RHE under illumination by a 6500 K Glacial White LED light source (Nexium). The Faradaic efficiency was estimated as the ratio between the measured concentration of evolved $Fe(CN)_6^{3-}$ in the electrolyte after photo-oxidation and that expected from the integrated charge transferred during the experiment if all of it was consumed by $Fe(CN)_6^{4-}$ oxidation. Concentration determination was done using Cary100 (Agilent).

Operando Raman Spectroelectrochemical Measurements. Raman measurements were done with a confocal Horiba LabRam HR evolution micro-Raman system, equipped with a Syncerity Open Electrode CCD detector (deep-cooled to—60 °C, 1024 × 256 pixels). The light source was a 633 nm laser at 12 mW on the sample in a reflectance mode. The laser was focused on the hematite surface with a ×50 objective, the measurements were taken using a 600 grooves/mm grating, and the confocal hole varied from 100 to 200 μm. The typical exposure time ranged from 50 to 150 s.

A specially designed PEC cell was used (Figure S9). Raman spectra were collected through the thin electrolyte layer (∼2.4 mm) with a Pt wire as a counter electrode and a Ag wire as a pseudo-reference electrode. Hematite deposited on the Pt/Silicon substrate was employed as the working electrode. Pt-coated silicon was chosen owing to its high reflectivity. An external laser was used as an excitation source (532 nm) at an intensity of ∼100 mW/cm^2 at the hematite surface. Constant potential was applied while measuring the Raman signal at the chronoamperometry mode of the potentiostat (VersaSTAT 4, Princeton Applied Research). To normalize the measured Raman spectra, the NaOH peak at 1066 cm^{-1} was taken as the standard peak as its intensity should be independent of potential, illumination conditions, hematite surface states, etc. Table S2 lists the experimental details of the operando Raman measurements. Raman spectra of the electrolytes (H_2O_2 and FeCN), i.e., unbiased and without catalyst (hematite), were measured by placing a drop of solution on a glass substrate and focusing close to the solution/air interphase.

ASSOCIATED CONTENT

Supporting Information

The Supporting Information is available free of charge at https://pubs.acs.org/doi/10.1021/acscatal.2c02849.

Linear and cyclic sweep voltammograms of H_2O_2 and FeCN in the dark and under constant and chopped illumination, details of the experimental setup and measurement conditions of operando Raman spectroelectrochemical measurements, and control experiments (PDF)

AUTHOR INFORMATION

Corresponding Author

Iris Visoly-Fisher − *Swiss Institute for Dryland Environmental and Energy Research, Blaustein Institutes for Desert Research, Ben-Gurion University of the Negev, Midreshet Ben-Gurion 8499000, Israel; Ilse Katz Institute for Nanoscale Science and Technology, Ben-Gurion University of the Negev, Be'er Sheva 8410501, Israel;* orcid.org/0000-0001-6058-4712; Email: irisvf@bgu.ac.il

Authors

Vivek Ramakrishnan − *Swiss Institute for Dryland Environmental and Energy Research, Blaustein Institutes for Desert Research, Ben-Gurion University of the Negev, Midreshet Ben-Gurion 8499000, Israel;* Present Address: Department of Chemistry, Sree Sankara College, Affiliated to Mahathma Gandhi University, Kalady, Ernakulam; orcid.org/0000-0002-0283-5525

Anton Tsyganok − *Department of Materials Science and Engineering, Technion − Israel Institute of Technology, Haifa 3200002, Israel*

Elena Davydova − *Department of Materials Science and Engineering, Technion − Israel Institute of Technology, Haifa 3200002, Israel*

Mariela J. Pavan − *Ilse Katz Institute for Nanoscale Science and Technology, Ben-Gurion University of the Negev, Be'er Sheva 8410501, Israel*

Avner Rothschild − *Department of Materials Science and Engineering and The Nancy & Stephen Grand Technion Energy Program (GTEP), Technion − Israel Institute of Technology, Haifa 3200002, Israel;* orcid.org/0000-0002-2512-0370

Complete contact information is available at: https://pubs.acs.org/10.1021/acscatal.2c02849

https://doi.org/10.1021/acscatal.2c02849
ACS Catal. 2023, 13, 540−549

Notes

The authors declare no competing financial interest.

■ ACKNOWLEDGMENTS

This research was supported by Israel's Ministry of Science and Technology grant #3-14423. A.R. acknowledges the support of the L. Shirley Tark Chair in Science and the Grand Technion Energy Program (GTEP). A.T. acknowledges the generous financial support by the Israel Ministry of Energy as a part of the scholarship program in the field of energy (219-01-044).

■ REFERENCES

(1) Tang, P.; Xie, H.; Ros, C.; Han, L.; Biset-Peiró, M.; He, Y.; Kramer, W.; Rodríguez, A. P.; Saucedo, E.; Galán-Mascarós, J. R.; Andreu, T.; Morante, J. R.; Arbiol, J. Enhanced photoelectrochemical water splitting of hematite multilayer nanowire photoanodes by tuning the surface state via bottom-up interfacial engineering. *Energy Environ. Sci.* **2017**, *10*, 2124−2136.

(2) Jeon, T. H.; Moon, G.-H.; Park, H.; Choi, W. Ultra-efficient and durable photoelectrochemical water oxidation using elaborately designed hematite nanorod arrays. *Nano Energy* **2017**, *39*, 211−218.

(3) Lohaus, C.; Klein, A.; Jaegermann, W. Limitation of Fermi level shifts by polaron defect states in hematite photoelectrodes. *Nat. Commun.* **2018**, *9*, 4309.

(4) Krumov, M. R.; Simpson, B. H.; Counihan, M. J. In situ quantification of surface intermediates and correlation to discharge products on hematite photoanodes using a combined scanning electrochemical microscopy approach. *Anal. Chem.* **2018**, *90*, 3050−3057.

(5) Takashima, T.; Ishikawa, K.; Irie, H. Detection of intermediate species in oxygen evolution on hematite electrodes using spectroelectrochemical measurements. *J. Phys. Chem. C* **2016**, *120*, 24827−24834.

(6) Le Formal, F.; Pendlebury, S. R.; Cornuz, M.; Tilley, S. D.; Grätzel, M.; Durrant, J. R. Back electron−hole recombination in hematite photoanodes for water splitting. *J. Am. Chem. Soc.* **2014**, *136*, 2564−2574.

(7) Grave, D. A.; Klotz, D.; Kay, A.; Dotan, H.; Gupta, B.; Visoly-Fisher, I.; Rothschild, A. Effect of Orientation on Bulk and Surface Properties of Sn-doped Hematite (α-Fe_2O_3) Heteroepitaxial Thin Film Photoanodes. *J. Phys. Chem. C* **2016**, *120*, 28961−28970.

(8) von Rudorff, G. F.; Jakobsen, R.; Rosso, K. M.; Blumberger, J. Fast Interconversion of Hydrogen Bonding at the Hematite (001)−Liquid Water Interface. *J. Phys. Chem. Lett.* **2016**, *7*, 1155−1160.

(9) Kennedy, J. H.; Frese, K. W. Photooxidation of Water at α-Fe_2O_3 Electrodes. *J. Electrochem. Soc.* **1978**, *125*, 709−714.

(10) Sivula, K.; Le Formal, F.; Grätzel, M. Solar Water Splitting: Progress Using Hematite (α-Fe_2O_3) Photoelectrodes. *ChemSusChem* **2011**, *4*, 432−449.

(11) Hayes, D.; Hadt, R. G.; Emery, J. D.; Cordones, A. A.; Martinson, A. B. F.; Shelby, M. L.; Fransted, K. A.; Dahlberg, P. D.; Hong, J.; Zhang, X.; Kong, Q.; Schoenlein, R. W.; Chen, L. X. Electronic and nuclear contributions to time-resolved optical and X-ray absorption spectra of hematite and insights into photoelectrochemical performance. *Energy Environ. Sci.* **2016**, *9*, 3754−3769.

(12) Grave, D. A.; Ellis, D. S.; Piekner, Y.; Kölbach, M.; Dotan, H.; Kay, A.; Schnell, P.; van de Krol, R.; Abdi, F. F.; Friedrich, D.; Rothschild, A. Extraction of mobile charge carrier photogeneration yield spectrum of ultrathin-film metal oxide photoanodes for solar water splitting. *Nat. Mater.* **2021**, *20*, 833−840.

(13) Piekner, Y.; Ellis, D. S.; Grave, D. A.; Tsyganok, A.; Rothschild, A. Wasted photons: photogeneration yield and charge carrier collection efficiency of hematite photoanodes for photoelectrochemical water splitting. *Energy Environ. Sci.* **2021**, *14*, 4584−4598.

(14) Klahr, B.; Gimenez, S.; Fabregat-Santiago, F.; Hamann, T.; Bisquert, J. Water Oxidation at Hematite Photoelectrodes: The Role of Surface States. *J. Am. Chem. Soc.* **2012**, *134*, 4294−4302.

(15) Dotan, H.; Sivula, K.; Grätzel, M.; Rothschild, A.; Warren, S. C. Probing the photoelectrochemical properties of hematite (α-Fe_2O_3) electrodes using hydrogen peroxide as a hole scavenger. *Energy Environ. Sci.* **2011**, *4*, 958−964.

(16) Corby, S.; Rao, R. R.; Steier, L.; Durrant, J. R. The kinetics of metal oxide photoanodes from charge generation to catalysis. *Nat. Rev. Mater.* **2021**, *6*, 1136−1155.

(17) Klahr, B.; Gimenez, S.; Fabregat-Santiago, F.; Bisquert, J.; Hamann, T. W. Electrochemical and photoelectrochemical investigation of water oxidation with hematite electrodes. *Energy Environ. Sci.* **2012**, *5*, 7626−7636.

(18) Klahr, B. M.; Hamann, T. W. Current and Voltage Limiting Processes in Thin Film Hematite Electrodes. *J. Phys. Chem. C* **2011**, *115*, 8393−8399.

(19) Klahr, B. M.; Martinson, A. B. F.; Hamann, T. W. Photoelectrochemical Investigation of Ultrathin Film Iron Oxide Solar Cells Prepared by Atomic Layer Deposition. *Langmuir* **2011**, *27*, 461−468.

(20) Klahr, B.; Gimenez, S.; Zandi, O.; Fabregat-Santiago, F.; Hamann, T. Competitive Photoelectrochemical Methanol and Water Oxidation with Hematite Electrodes. *ACS Appl. Mater. Interfaces* **2015**, *7*, 7653−7660.

(21) Avital, Y. Y.; Dotan, H.; Klotz, D.; Grave, D. A.; Tsyganok, A.; Gupta, B.; Kolusheva, S.; Visoly-Fisher, I.; Rothschild, A.; Yochelis, A. Two-site H_2O_2 photo-oxidation on haematite photoanodes. *Nat. Commun.* **2018**, *9*, 4060.

(22) Zandi, O.; Hamann, T. W. Determination of photoelectrochemical water oxidation intermediates on haematite electrode surfaces using operando infrared spectroscopy. *Nat. Chem.* **2016**, *8*, 778−783.

(23) Busch, M. Water oxidation: From mechanisms to limitations. *Curr. Opin. Electrochem.* **2018**, *9*, 278−284.

(24) Li, J.; Wan, W.; Triana, C. A.; Chen, H.; Zhao, Y.; Mavrokefalos, C. K.; Patzke, G. R. Reaction kinetics and interplay of two different surface states on hematite photoanodes for water oxidation. *Nat. Commun.* **2021**, *12*, 255.

(25) Bai, L.; Lee, S.; Hu, X. Spectroscopic and Electrokinetic Evidence for a Bifunctional Mechanism of the Oxygen Evolution Reaction. *Angew. Chem., Int. Ed.* **2021**, *60*, 3095−3103.

(26) Mesa, C. A.; Francàs, L.; Yang, K. R.; Garrido-Barros, P.; Pastor, E.; Ma, Y.; Kafizas, A.; Rosser, T. E.; Mayer, M. T.; Reisner, E.; Grätzel, M.; Batista, V. S.; Durrant, J. R. Multihole water oxidation catalysis on haematite photoanodes revealed by operando spectroelectrochemistry and DFT. *Nat. Chem.* **2020**, *12*, 82−89.

(27) Tsyganok, A.; Ghigna, P.; Minguzzi, A.; Naldoni, A.; Murzin, V. Y.; Caliebe, W.; Rothschild, A.; Ellis, D. S. Operando X-ray absorption spectroscopy (XAS) observation of photoinduced oxidation in FeNi (oxy) hydroxide overlayers on hematite (α-Fe_2O_3) photoanodes for solar water splitting. *Langmuir* **2020**, *36*, 11564−11572.

(28) Mesa, C. A.; Kafizas, A.; Francàs, L.; Pendlebury, S. R.; Pastor, E.; Ma, Y.; Le Formal, F.; Mayer, M. T.; Grätzel, M.; Durrant, J. R. Kinetics of Photoelectrochemical Oxidation of Methanol on Hematite Photoanodes. *J. Am. Chem. Soc.* **2017**, *139*, 11537−11543.

(29) Hedenstedt, K.; Bäckström, J.; Ahlberg, E. In-situ Raman spectroscopy of α-and γ-FeOOH during cathodic load. *J. Electrochem. Soc.* **2017**, *164*, H621.

(30) Louie, M. W.; Bell, A. T. An Investigation of Thin-Film Ni−Fe Oxide Catalysts for the Electrochemical Evolution of Oxygen. *J. Am. Chem. Soc.* **2013**, *135*, 12329−12337.

(31) Yeo, B. S.; Bell, A. T. Enhanced Activity of Gold-Supported Cobalt Oxide for the Electrochemical Evolution of Oxygen. *J. Am. Chem. Soc.* **2011**, *133*, 5587−5593.

(32) Pasquini, C.; D'Amario, L.; Zaharieva, I.; Dau, H. Operando Raman spectroscopy tracks oxidation-state changes in an amorphous Co oxide material for electrocatalysis of the oxygen evolution reaction. *J. Chem. Phys.* **2020**, *152*, 194202.

(33) Pavlovic, Z.; Ranjan, C.; van Gastel, M.; Schlögl, R. The active site for the water oxidising anodic iridium oxide probed through in situ Raman spectroscopy. *Chem. Commun.* **2017**, *53*, 12414−12417.

(34) Joya, K. S.; de Groot, H. J. M. Electrochemical in situ surface enhanced Raman spectroscopic characterization of a trinuclear ruthenium complex, Ru-red. *J. Raman Spectrosc.* **2013**, *44*, 1195−1199.
(35) Joya, K. S.; Sala, X. In situ Raman and surface-enhanced Raman spectroscopy on working electrodes: spectroelectrochemical characterization of water oxidation electrocatalysts. *Phys. Chem. Chem. Phys.* **2015**, *17*, 21094−21103.
(36) Cho, K. H.; Park, S.; Seo, H.; Choi, S.; Lee, M. Y.; Ko, C.; Nam, K. T. Capturing Manganese Oxide Intermediates in Electrochemical Water Oxidation at Neutral pH by In Situ Raman Spectroscopy. *Angew. Chem., Int. Ed.* **2021**, *60*, 4673−4681.
(37) Bo, X.; Li, Y.; Chen, X.; Zhao, C. Operando Raman Spectroscopy Reveals Cr-Induced-Phase Reconstruction of NiFe and CoFe Oxyhydroxides for Enhanced Electrocatalytic Water Oxidation. *Chem. Mater.* **2020**, *32*, 4303−4311.
(38) Radinger, H.; Connor, P.; Stark, R.; Jaegermann, W.; Kaiser, B. Manganese Oxide as an Inorganic Catalyst for the Oxygen Evolution Reaction Studied by X-Ray Photoelectron and Operando Raman Spectroscopy. *ChemCatChem* **2021**, *13*, 1175−1185.
(39) Chen, Z.; Cai, L.; Yang, X.; Kronawitter, C.; Guo, L.; Shen, S.; Koel, B. E. Reversible Structural Evolution of NiCoOxHy during the Oxygen Evolution Reaction and Identification of the Catalytically Active Phase. *ACS Catal.* **2018**, *8*, 1238−1247.
(40) Páez, T.; Martínez-Cuezva, A.; Palma, J.; Ventosa, E. Revisiting the cycling stability of ferrocyanide in alkaline media for redox flow batteries. *J. Power Sources* **2020**, *471*, No. 228453.
(41) De Faria, D.; Venâncio Silva, S.; De Oliveira, M. Raman microspectroscopy of some iron oxides and oxyhydroxides. *J. Raman Spectrosc.* **1997**, *28*, 873−878.
(42) de Faria, D. L. A.; Lópes, F. N. Heated goethite and natural hematite: can Raman spectroscopy be used to differentiate them? *Vib. Spectrosc.* **2007**, *45*, 117−121.
(43) Malviya, K. D.; Dotan, H.; Shlenkevich, D.; Tsyganok, A.; Mor, H.; Rothschild, A. Systematic comparison of different dopants in thin film hematite (α-Fe_2O_3) photoanodes for solar water splitting. *J. Mater. Chem. A* **2016**, *4*, 3091−3099.
(44) Xu, M.; Wang, Z.; Xu, Q.; Song, Q.; You, J.; Zhai, Y. An in situ spectroscopic study on decomposition of $MgSiO_3$ during the alkali fusion process using sodium hydroxide. *New J. Chem.* **2014**, *38*, 1528−1532.
(45) Bonin, P. M.; Jędral, W.; Odziemkowski, M. S.; Gillham, R. W. Electrochemical and Raman spectroscopic studies of the influence of chlorinated solvents on the corrosion behaviour of iron in borate buffer and in simulated groundwater. *Corros. Sci.* **2000**, *42*, 1921−1939.
(46) Trolard, F.; Génin, J.-M.; Abdelmoula, M.; Bourrié, G.; Humbert, B.; Herbillon, A. Identification of a green rust mineral in a reductomorphic soil by Mossbauer and Raman spectroscopies. *Geochim. Cosmochim. Acta* **1997**, *61*, 1107−1111.
(47) Legrand, L.; Sagon, G.; Lecomte, S.; Chausse, A.; Messina, R. A Raman and infrared study of a new carbonate green rust obtained by electrochemical way. *Corros. Sci.* **2001**, *43*, 1739−1749.
(48) Lanneluc, I.; Langumier, M.; Sabot, R.; Jeannin, M.; Refait, P.; Sablé, S. On the bacterial communities associated with the corrosion product layer during the early stages of marine corrosion of carbon steel. *Int. Biodeterior. Biodegrad.* **2015**, *99*, 55−65.
(49) Refait, P.; Nguyen, D.; Jeannin, M.; Sable, S.; Langumier, M.; Sabot, R. Electrochemical formation of green rusts in deaerated seawater-like solutions. *Electrochim. Acta* **2011**, *56*, 6481−6488.
(50) Abdelmoula, M.; Refait, P.; Drissi, S.; Mihe, J.; Génin, J.-M. Conversion electron Mössbauer spectroscopy and X-ray diffraction studies of the formation of carbonate-containing green rust one by corrosion of metallic iron in $NaHCO_3$ and ($NaHCO_3^+$ NaCl) solutions. *Corros. Sci.* **1996**, *38*, 623−633.
(51) Rennert, T.; Mansfeldt, T. Sorption of iron-cyanide complexes on goethite. *Eur. J. Soil Sci.* **2001**, *52*, 121−128.
(52) Rennert, T.; Mansfeldt, T. Sorption of iron−cyanide complexes on goethite in the presence of sulfate and desorption with phosphate and chloride. *J. Environ. Qual.* **2002**, *31*, 745−751.
(53) Rennert, T.; Mansfeldt, T. Iron-cyanide complexes in soil under varying redox conditions: speciation, solubility and modelling. *Eur. J. Soil Sci.* **2005**, *56*, 527−536.
(54) Ahlinder, L.; Ekstrand-Hammarström, B.; Geladi, P.; Österlund, L. Large uptake of titania and iron oxide nanoparticles in the nucleus of lung epithelial cells as measured by Raman imaging and multivariate classification. *Biophys. J.* **2013**, *105*, 310−319.
(55) De la Fuente, D.; Alcántara, J.; Chico, B.; Díaz, I.; Jiménez, J.; Morcillo, M. Characterisation of rust surfaces formed on mild steel exposed to marine atmospheres using XRD and SEM/Micro-Raman techniques. *Corros. Sci.* **2016**, *110*, 253−264.
(56) Maghémite. Available from: https://commons.wikimedia.org/wiki/File:Crystal_structure_of_green_rust.svg.
(57) Tsyganok, A.; Monroy-Castillero, P.; Piekner, Y.; Yochelis, A.; Rothschild, A. Parallel water photo-oxidation reaction pathways in hematite photoanodes: implications for solar fuel production. *Energy Environ. Sci.* **2022**, *15*, 2445−2459.
(58) Valdés, Á.; Brillet, J.; Grätzel, M.; Gudmundsdóttir, H.; Hansen, H. A.; Jónsson, H.; Klüpfel, P.; Kroes, G. -J.; Le Formal, F.; Man, I. C.; Martins, R. S.; Nørskov, J. K.; Rossmeisl, J.; Sivula, K.; Vojvodic, A.; Zäch, M. Solar hydrogen production with semiconductor metal oxides: new directions in experiment and theory. *Phys. Chem. Chem. Phys.* **2012**, *14*, 49−70.
(59) Poaty, L. T.; Ulman, K.; Seriani, N.; M'Passi-Mabiala, B.; Gebauer, R. Characterization of peroxo reaction intermediates in the water oxidation process on hematite surfaces. *J. Mol. Model.* **2018**, *24*, 284.
(60) Yatom, N.; Neufeld, O.; Caspary Toroker, M. Toward settling the debate on the role of Fe_2O_3 surface states for water splitting. *J. Phys. Chem. C* **2015**, *119*, 24789−24795.
(61) Cowan, A. J.; Barnett, C. J.; Pendlebury, S. R.; Barroso, M.; Sivula, K.; Grätzel, M.; Durrant, J. R.; Klug, D. R. Activation energies for the rate-limiting step in water photooxidation by nanostructured α-Fe_2O_3 and TiO_2. *J. Am. Chem. Soc.* **2011**, *133*, 10134−10140.
(62) Le Formal, F.; Pastor, E.; Tilley, S. D.; Mesa, C. A.; Pendlebury, S. R.; Grätzel, M.; Durrant, J. R. Rate law analysis of water oxidation on a hematite surface. *J. Am. Chem. Soc.* **2015**, *137*, 6629−6637.
(63) Boehme, K.; Brauer, H. D. Generation of singlet oxygen from hydrogen peroxide disproportionation catalyzed by molybdate ions. *Inorg. Chem.* **1992**, *31*, 3468−3471.
(64) George, K.; Khachatrjan, T.; van Berkel, M.; Sinha, V.; Bieberle-Hütter, A. Understanding the Impact of Different Types of Surface States on Photoelectrochemical Water Oxidation: A Microkinetic Modeling Approach. *ACS Catal.* **2020**, *10*, 14649−14660.
(65) Peter, L. M.; Wijayantha, K. G. U.; Tahir, A. A. Kinetics of light-driven oxygen evolution at α-Fe_2O_3 electrodes. *Faraday Discuss.* **2012**, *155*, 309−322.

https://doi.org/10.1021/acscatal.2c02849
ACS Catal. 2023, 13, 540−549